Supplementary Materials for

Correlative x-ray phase-contrast tomography and histology of human brain tissue affected by Alzheimer's disease

Mareike Töpperwien, Franziska van der Meer, Christine Stadelmann, Tim Salditt

	laboratory	GINIX setup
energy (keV)	0-40/9.25	8
$z_{01,\mathrm{min}}$ (mm)	158.75	145
$z_{01} + z_{12}$ (m)	0.186	5.05
p_{eff} (nm)	461	187
field of view (μm^2)	1152×1530	383×383
number of distances	1	4
angular range (°)	[0,180]	[0,180]
number of projections	1000	1500
exposure time (s)	50	0.1
BAC α	0.01	-
BAC $(\gamma \cdot F)$	0.15	-
CTF δ/β	-	50
CTF α_2	-	0

Table S1: Experimental parameters used for imaging of a 1 mm punch from a paraffin-embedded human AD hippocampus.

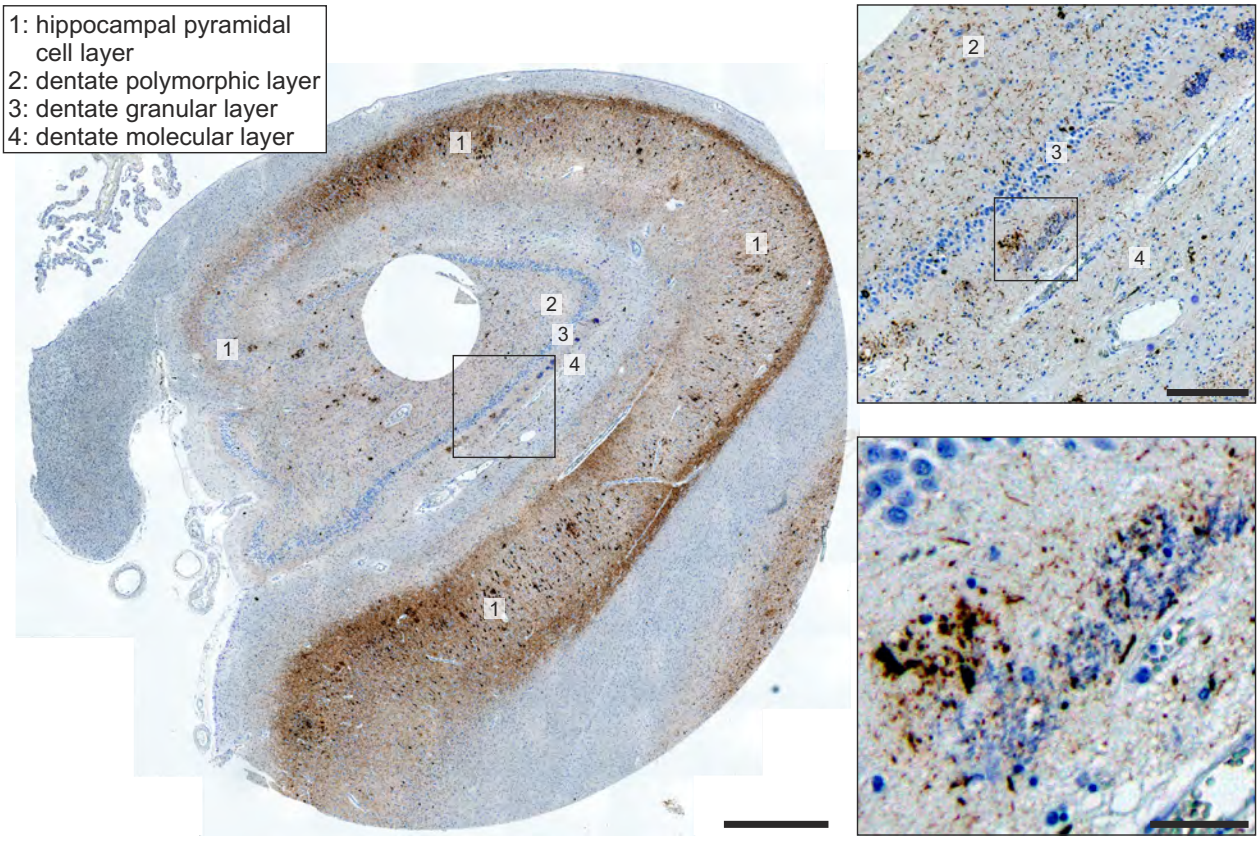

Figure S1: Histological section of the entire hippocampus, stained with a Tau antibody and hematoxylin. The different parts of the hippocampus, namely the pyramidal cell layer as well as the granular, molecular and polymorphic layer of the dentate gyrus can be well recognized. Neurofibrillary tangles and senile plaques, typical hallmarks of Alzheimer's disease, are also visible throughout the entire hippocampus. The circular hole within the section indicates the position of the biopsy punch considered in the main manuscript. The magnified regions on the right show the presence of amyloid plaques in the dentate molecular layer in close proximity to the granular layer. Note that both unaffected as well as mineralized plaques, further considered in the main manuscript, can be distinguished due to the different staining protocols, resulting in Tau-positive senile plaques appearing brown as well as mineralized plaques, which are mainly hematoxylin-positive and hence appear blue but also contain to some extent Tau-positive structures. Note that the contrast has been adjusted to ensure maximum visibility of the features of interest. Scale bars: 1 mm (left), 200 µm (right, top) and 50 µm (right, bottom)

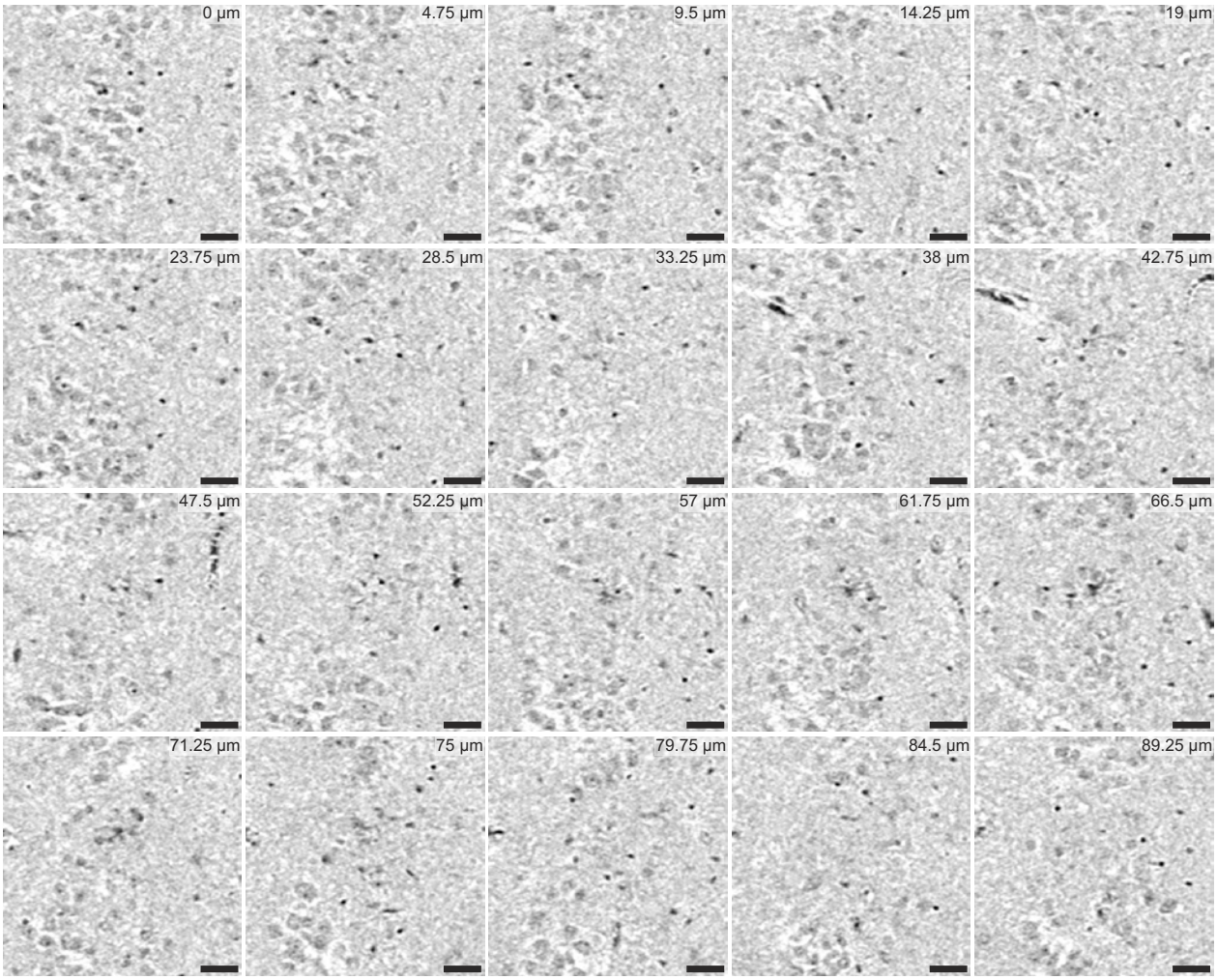

Figure S2: Appearance of a senile plaque without calcifications in several consecutive virtual slices. Note that the relative position of the slice with respect to the first is indicated in the upper right corner. The plaque under consideration is the upper one shown in the left panels of Fig. 3 in the main text which was visualized via a Tau antibody stain. Within the virtual slices from the tomographic scan it is mainly visible due to the missing cells in the band of the granular layer, showing that the plaque itself does not comprise a significantly higher electron density compared to the surrounding tissue. Within the plaque region, structural alterations, which could possibly be associated with the β-amyloid protein, as well as an accumulation of small cells, which can be identified as microglia (cf. Fig. S6 and S7), can be observed. This accumulation of microglia could act as an indirect marker for amyloid plaques in unstained human tissue. Scale bars: 30 µm

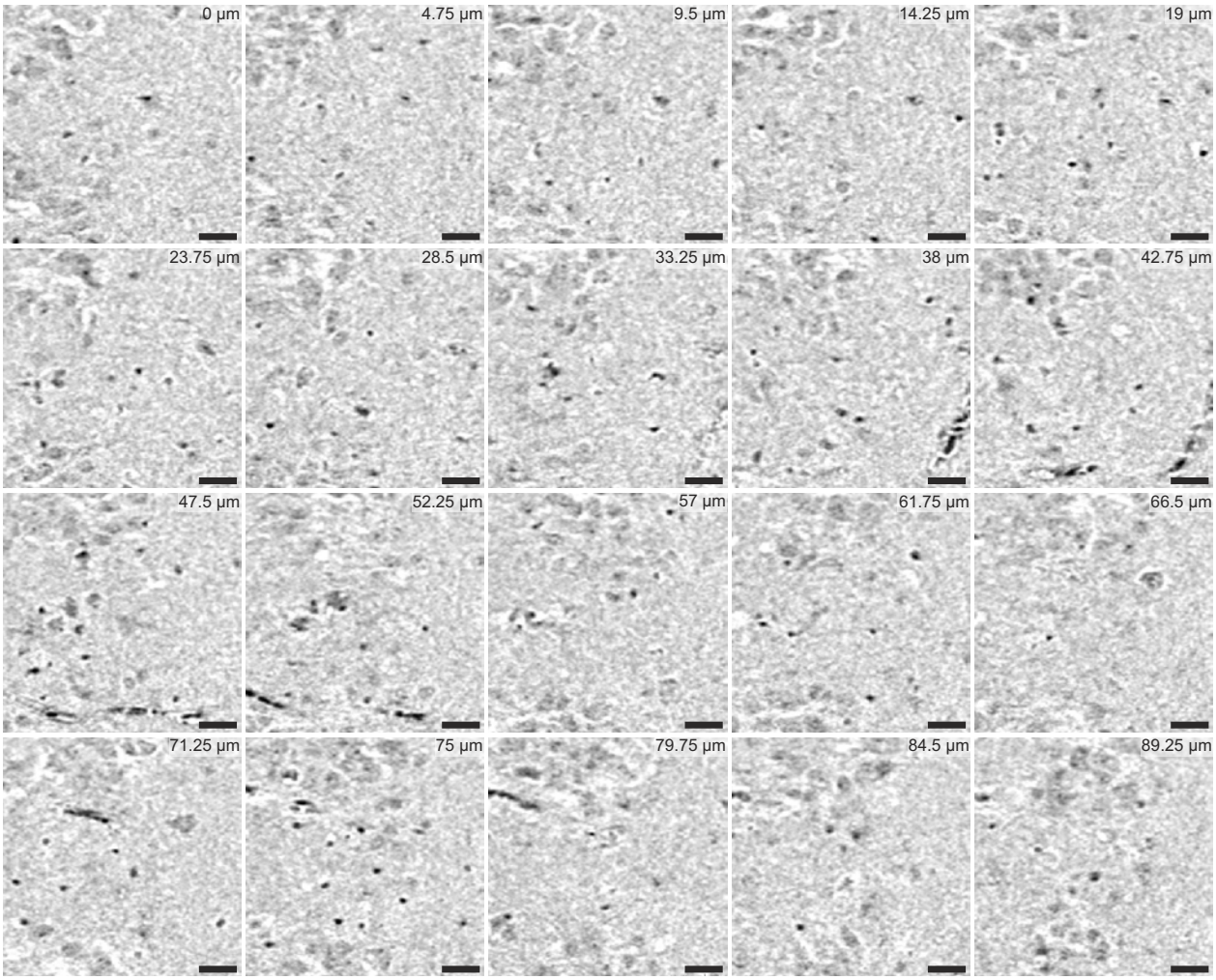

Figure S3: Appearance of a second senile plaque within the results of the tomographic scan. In this case, the plaque under consideration is the lower one from the left panels of Fig. 3 in the main text. Again, the plaque is mainly visible due to the missing cells in the band of the granular layer. Also in this case, structural alterations within the tissue as well as a relatively large number of small cells can be observed in the vicinity of the plaque, indicating that this might be an alternative marker for the presence of senile plaques in human tissue. Scale bars: 25 µm

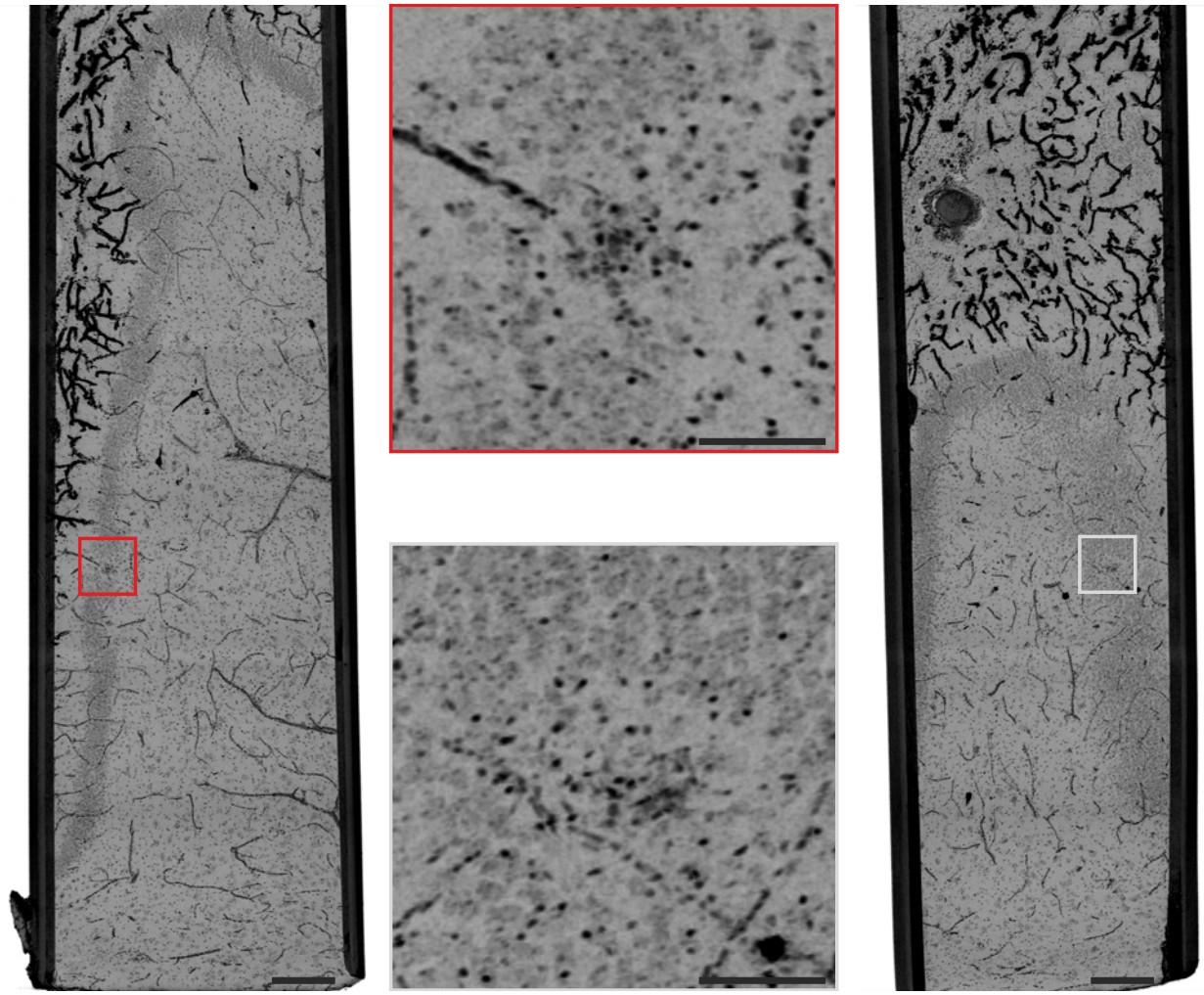

Figure S4: Maximum intensity projections within the region of a senile plaque. The maximum intensity projections were carried out over 60 consecutive slices within the region of the senile amyloid plaque shown in Fig. S2 from two orthogonal directions. The magnified views in the center correspond to the regions marked by the rectangles in the large overviews on the left and right, respectively. In this representation the accumulation of microglia in the plaque area can be well recognized whereas the plaque itself remains invisible as it does not have a larger electron density compared to the surrounding tissue. Scale bars: 200 µm (overviews) and 50 µm (magnified views)

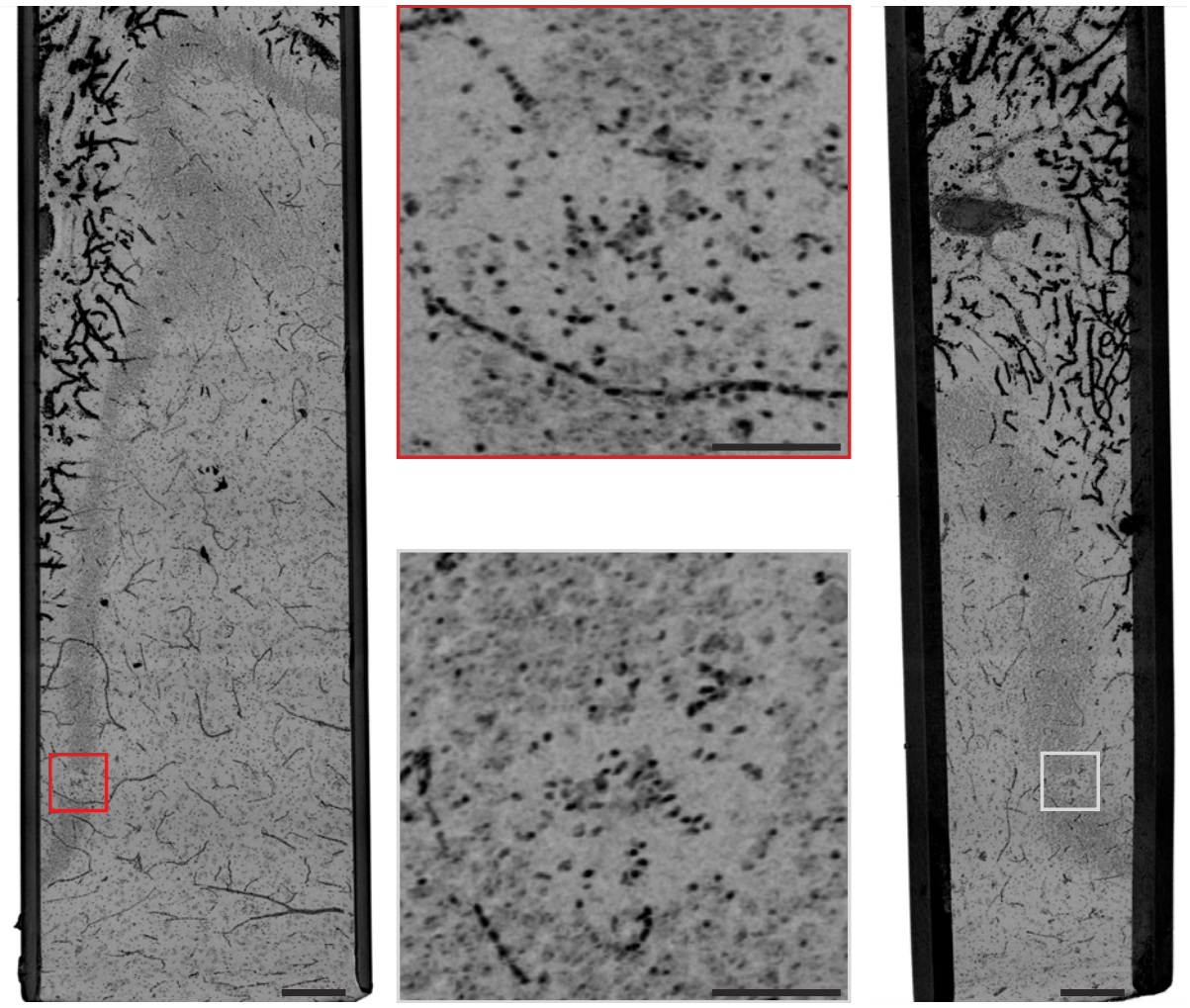

Figure S5: Maximum intensity projections within the region of a second senile plaque. The maximum intensity projections were carried out over 60 consecutive slices within the region of the senile amyloid plaque shown in Fig. S3 from two orthogonal directions, again visualizing the accumulation of microglia in the vicinity of the plaque. Scale bars: 200 µm (overviews) and 50 µm (magnified views)

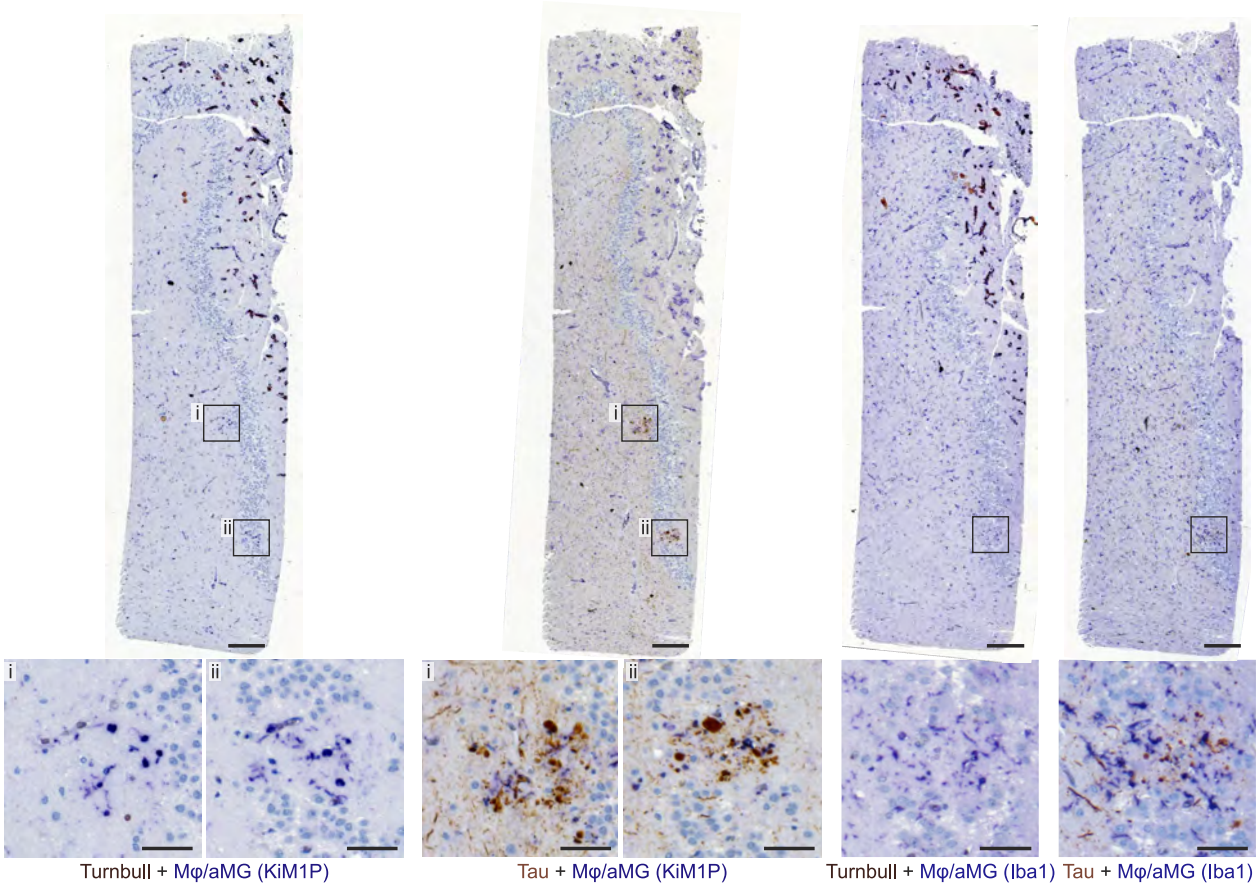

Figure S6: Distribution of microglia in the vicinity of the senile plaques without calcifications. In addition to the staining protocols used for the slices shown in Fig. 3 in the main manuscript, namely the Turnbull protocol for iron, a Tau antibody stain for the Alzheimer pathology and hematoxylin for cell nuclei and calcified material, immunohistochemistry was performed on the same sections for KiM1P as well as Iba1, both acting as markers for macrophages/activated microglia (Mφ/aMG). Hence, iron-positive structures appear dark brown/black (mainly mineralized blood vessels in the dentate molecular layer), Tau-positive structures brown, cells and calcified material light blue and Mφ/aMG dark blue. While both staining methods for Mφ/aMG reveal that these cells exist throughout the tissue, a clear accumulation can be observed within the regions occupied by the senile plaques. Since other cells such as the dentate granule cells are missing in this region, the small cells, which can be found within the plaque region in the µCT results shown in Figs. S2 and S3, can be identified as microglia or rather their electron-dense nuclei (cf. Fig. S7 for a one-to-one comparison). Note that the contrast has been adjusted to ensure maximum visibility of the features of interest. Scale bars: 200 µm (top) and 50 µm (bottom)

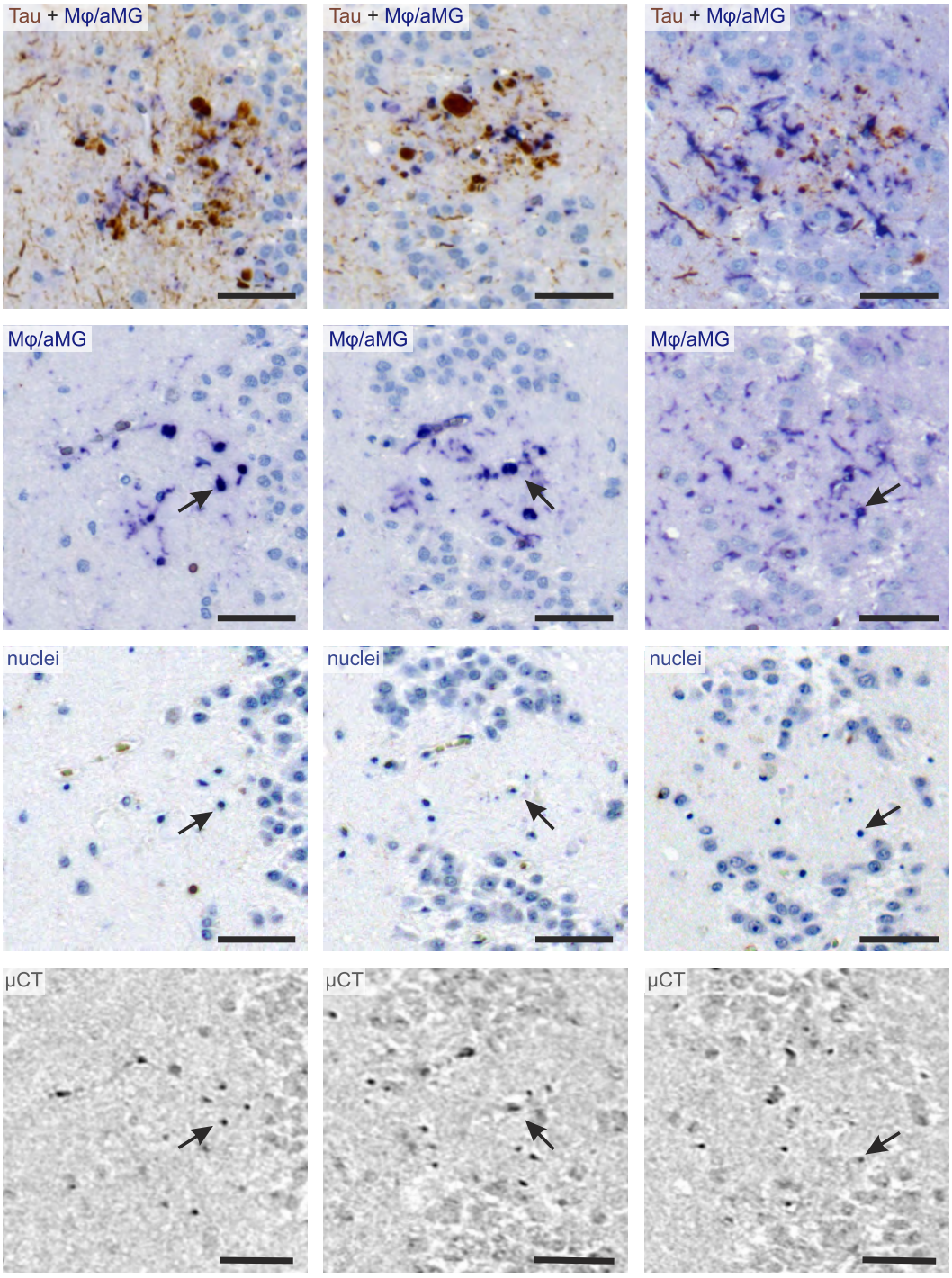

Figure S7: Comparison between virtual slices through the µCT results and histological sections stained for macrophages/activated microglia (Mφ/aMG). Additionally, Tau protein as well as cell nuclei are visualized, the latter via a hematoxylin counterstain. Note that the µCT slices are not exactly the same as in Fig. 3 in the main manuscript as in this case the alignment was focused on the microglia and not the mineralized blood vessels. The comparison clearly shows the consistency between the histological sections and the µCT results, as indicated by the arrows pointing towards exemplary microglia, proving that the small electron-dense structures in the latter are indeed microglia or rather their nuclei. Scale bars: 50 µm